Journal of Alloys and Compounds 509 (2011) 961–965

Contents lists available at ScienceDirect

Journal of Alloys and Compounds

journal homepage: www.elsevier.com/locate/jallcom

Facile synthesis of ZnO nanobullets/nanoflakes and their applications to dye-sensitized solar cells

Jixia Mou [a], Weiguang Zhang [a,*], Jun Fan [a], Hong Deng [a], Wei Chen [b]

[a] School of Chemistry & Environment, South China Normal University, Guangzhou 510006, China
[b] Wuhan National Laboratory for Optoelectronics and College of Optoelectronic Science and Engineering, Huazhong University of Science and Technology, Wuhan 430074, China

ARTICLE INFO

Article history:
Received 26 April 2010
Received in revised form
19 September 2010
Accepted 22 September 2010
Available online 20 October 2010

Keywords:
Hydro/solvothermal reaction
ZnO nanostructures
Photoanodes
Dye-sensitized solar cells

ABSTRACT

In this paper we reported a successful synthesis of ZnO nanobullets/nanoflakes by a simple hydro/solvothermal method employing a mixture of water/ethylene glycol as the solvent, and zinc acetate as the zinc source. The final products were characterized by powder X-ray diffraction, scanning electron microscopy and transmission electron microscopy. Raman scattering and photofluorescence spectra of the products were also investigated. ZnO with both nanobullets and nanoflakes nanostructures had been comparably studied as active photoanodes in dye-sensitized solar cell (DSSC) system, and the overall light-to-energy conversion efficiency of 1.93% has been achieved for nanobullets based DSSC, while that for ZnO nanoflakes based DSSC has been raised up to 3.64%.

1. Introduction

The controlled growth of ZnO nanostructures has attracted considerable attention during the past few decades because of their novel properties of semiconductors depending on their different sizes, shapes and structures [1–5]. ZnO can be easily processed into various nanostructures due to its nature in chemistry. To date, numerous ZnO nanostructures with different sizes and morphologies such as nanowires [6–12], nanorods [13–15], nanotubes [16], nanotetrapods [17], nanosheet [18] and nanodisks [19], have been successfully synthesized through different methods. As an inorganic semiconducting material, the noncentrosymmetric wurtzite ZnO semiconductor has a wide band-gap (3.37 eV) and a large exciton binding energy (60 meV), which becomes one of the most important functional materials with unique photoelectric properties of near-UV emission, optical transparency, electric conductivity, and piezoelectricity, and has also been widely investigated in the potential applications of nanodevices, such as field-effect transistors, lasers, photodiodes, chemical and biological sensors, and solar cells [20–26].

Dye-sensitized solar cell (DSSC) is regarded as one of the most promising candidates in photovoltaics in the last two decades [27–32]. ZnO is an effective n-type semiconductor material, which has been explored in this field with great potential [33–42]. Recently, Zhang et al. reported polydisperse ZnO aggregates based DSSCs, which achieved an overall energy conversion efficiency up to 5.4% [33,34]. And later, Qiu et al. prepared a superstructure of meso/micro-porous single-crystalline ZnO nanoplates, which was fabricated as a photoanode of DSSC and an efficiency of 5% was reached [36].

Although there are many available methods to fabricate ZnO nanostructures, we report here a simple and generalized method to prepare ZnO nanocrystallites from zinc acetates by adjusting the volume ratio between water and ethylene glycol solvents. In comparison, this synthetic method is of relatively low cost and can be readily scaled-up for industrial production. Although ZnO bullets have been recently synthesized by some researchers [43], the diameters of the hexagonal base achieved so far are larger than 500 nm and the lengths are longer than 1 μm. The ZnO bullets in our synthetic approach are able to be prepared with the diameters of hexagonal base down to 50 nm and the lengths ranging from 100 nm to 300 nm. Interestingly, ultrathin ZnO nanoflake was prepared from thermal decomposition of a flake-like precursor that was obtained from the solvothermal treatment of zinc acetate dihydrate and ethylene glycol. The ultrathin ZnO nanoflake was applied as photoanode material of DSSC, and an overall energy conversion efficiency of 3.64% was achieved under 100 mW/cm^2 light intensity, making it promising candidate for the development of novel DSSCs.

* Corresponding author. Tel.: +86 20 39310210; fax: +86 20 39310187.
E-mail address: wgzhang@scnu.edu.cn (W. Zhang).

0925-8388/$ – see front matter © 2010 Elsevier B.V. All rights reserved.
doi:10.1016/j.jallcom.2010.09.148

2. Experimental procedures

2.1. Materials and characterization

All the chemical reagents, such as zinc acetate dihydrate ($Zn(Ac)_2{\cdot}2H_2O$), ethylene glycol are of analytical grade, were used without further treatment for the preparation of ZnO nanomaterials. The as-prepared products were characterized by scanning electron microscopy (SEM), transmission electron microscopy (TEM) and powder X-ray diffraction (XRD) measurements. The morphologies were directly examined by SEM using a JEOL 6700F at an accelerating voltage of 5 kV. TEM observations were carried out on JEOL 2010 microscopes operating at 200 kV. The XRD analysis was performed on a Philips PW-1830 X-ray diffractometer with Cu Ka radiation (λ = 1.5406 Å) at a scanning speed of 0.025°/s over the 2θ range of 10–70°. Film thickness was detected by a Tencor Alpha-Step 200 surface profiler system. Each film thickness was confirmed by repeating tests for three times. BET surface area was characterized using a Coulter SA 3100 surface area analyzer. The fluorescence spectra were measured using a Perkin-Elmer LS-55 spectrofluorimeter equipped with a pulsed xenon lamp as light source.

2.2. Preparation of ZnO nanobullets and nanoflakes

A typical procedure was as follows: for ZnO nanobullets synthesis, 2 mmol of zinc acetate dihydrate was dissolved in 10 mL of water with magnetic stirring for 15 min. 20 mL of ethylene glycol was added into the above solution with magnetic stirring for 30 min. Then the mixture was sealed in a Teflon-lined stainless-steel autoclave of 50 mL capacity, and kept at 150 °C for 10 h. The product hereafter is denoted as sample 1. For ZnO nanoflakes synthesis, zinc acetate dihydrate (1 mmol) was dissolved in ethylene glycol (30 mL) only. Then the mixture was sealed in a Teflon-lined stainless-steel autoclave of 50 mL capacity, and kept at 130 °C for 10 h. The autoclaves were allowed to cool down to room temperature naturally. White precipitates were centrifugally collected, rinsed with absolute ethanol several times and dried in air overnight. Finally, the precipitates of the flake-like precursor was heated to 400 °C and kept for 1 h in oxygen atmosphere. This product hereafter was denoted as sample 2.

2.3. Fabrication of the ZnO photoelectrode films and performance measurements

The as-prepared colloidal solution of sample 1 was concentrated by centrifugal separation. Then the concentrated solution was heated to obtain a homogenous paste with certain viscosity. While for the preparation of photoanodes based on sample 2, the as-prepared precursor was first ground in an agate mortar and then was dispersed in a little amount of water to form a homogenous paste. The pastes were spread on FTO glass by doctor blade technique using adhesive tape as the spacer. After the films were dried, they were annealed at 400 °C for 1 h to remove the residual organic matter from the ZnO surface. The ZnO photoanodes were then immersed in a 0.3 mM ethanol solution of N719 dye (cis-bis(isothiocyanato)bis(2,2′-bipyridyl-4,4′-dicarboxylato)-ruthenium(II) bis-tetrabutylammonium, Dyesol, Australia) in a closed bottle for 2 h. The electrolyte composition was 0.5 M tetra-butylammonium iodide, 0.1 M lithium iodide, 0.1 M iodine, and 0.5 M 4-tert-butyl pyridine in an acetonitrile and valeronitrile mixed solvent (85/15 by volume). A conductive glass sputter-coated with 100 nm of Pt was used as the counter-electrode. The electrodes were sandwiched with a 25 μm thick Surlyn hot-melt gasket. The photocurrent–photovoltage (J–V) characteristic curves were recorded using a computerized Keithley 236 source measure unit. The light source (Oriel solar simulator, 450 W, AM 1.5 global filter) was calibrated to be 1 sun (100 mW/cm^2) using a power meter. The active electrode area was typically 0.16 cm^2.

3. Results and discussion

Crystal phase compositions of the as-synthesized products were identified by XRD patterns. As shown in Fig. 1, sample 1 and sample 2 possess similar XRD patterns. All strong peaks can be indexed as the pure hexagonal phase of wurtzite-type ZnO (space group: P63mc) with lattice constants a = 3.25 Å and c = 5.21 Å, in agreement with the reported data (JCPDS no. 79-0206). The sharp and strong peaks of both sample 1 and sample 2 confirm that both are well crystallized and with high purity.

Fig. 2(a) shows the low magnification SEM image of sample 1. It reflects that the product has a bullet-like morphology with the diameter of the hexagonal base ranging from 50 to 100 nm and the length from 100 to 300 nm. To catch the more detail about the morphological characteristics of the bullet-like ZnO nanostructure, a representative high magnification SEM image was shown in the inset of Fig. 2(a), which reflects the product with a pyramidal structure. The as-synthesized ZnO nanobullet was further investigated by TEM and Energy-dispersive X-ray (EDX) spectroscopy.

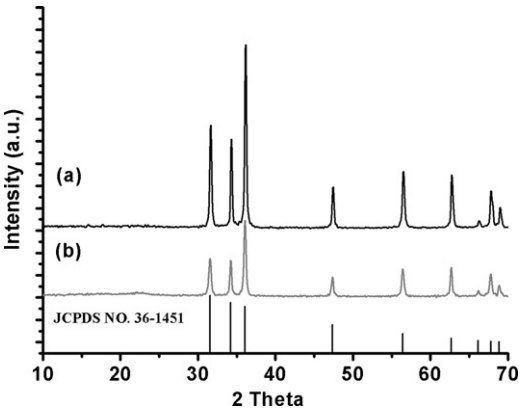

Fig. 1. XRD patterns of sample 1 (a) and sample 2 (b).

A representative TEM image of the ZnO nanobullets is shown in Fig. 2(b). It can be seen that they are tapering by decreasing diameter. Interestingly, the nanobullets have rough surface and appear to be hierarchically assembled from three or four nanoparticles. EDX analysis in the inset of Fig. 2(b) taken on an individual nanobullet shows the existence of only Zn and O excluding the Cu signal came from the copper TEM grid. A corresponding high magnification HRTEM image in the Fig. 2(c) exhibits clear lattice fringes; the lattice spacing of 2.6 Å is recognized and can be ascribed to the (0 0 2) planes of the hexagonal phase of ZnO. Fig. 2(d) shows its corresponding SAED pattern taken from the nanobullet, indicating a plausibly mesocrystalline nature of the nanobullet.

During the fabrication process of sample 2, it has been confirmed by XRD pattern that the solvothermal treatment of zinc acetate dihydrate and ethylene glycol cannot form crystalline ZnO. Only after annealing at 400 °C for 1 h, the amorphous precursor was transformed into crystalline phase (see Fig. 1(b)). Shown in Fig. 3(a) and (b) is SEM images of sample 2 after annealing. The product has a flake-shaped morphology. The flake-shaped structure is more than 500 nm in width and about 10 nm in thickness. The ZnO nanoflakes were further investigated by TEM, and high-resolution transmission electron microscopy (HRTEM). As shown in Fig. 3(c), the ZnO nanoflake is ultrathin due to the curliness of its edge. As its corresponding HRTEM image in Fig. 3(d) shows, the ZnO nanoflake exhibits clear lattice fringes with the lattice spacing of 0.26 and 0.24 nm, corresponding to the (0 0 2) and (1 1 1) lattice spacings of a hexagonal ZnO crystal, respectively. It suggests that they are well-crystallized single crystals, consistent with the XRD analysis. The fast Fourier transform (FFT) pattern from the inset of Fig. 3(d) is in good agreement with the diffraction pattern of the [0 0 1] zone axis in ZnO.

On the basic of above results, the growth mechanism of different nanostructured ZnO can be discussed as follows. The polar crystal of ZnO nanostructure grows preferentially along [0 0 1] direction because of the lowest surface energy of (0 0 1) facet. The growth velocity along ⟨1 0 1⟩ directions is slower than that along [0 0 1] direction, so that the pillar morphology is often obtained. Meanwhile, the growth of ZnO along [0 0 1] direction may be accelerated or suppressed in hydro/solvothermal system as having or lacking oxygen and hydroxyl OH^-. For example, short pillar and particles structures can be achieved in solvent of glycol lacking hydroxyl OH^- [44–46]. In this study, the growth units of $[Zn(OH)_4]^{2-}$ generated by zinc ions and water prefer to be adsorbed on the positive polar plane by coulomb interactions, as a result, further nucleation takes place along this direction. In the growth process, the little amount of water is slowly expended, which results in the growth of the tapered pillar morphology. For the growth of flake-shaped structure, the growth units of $[Zn(OH)_4]^{2-}$ are rare due to water

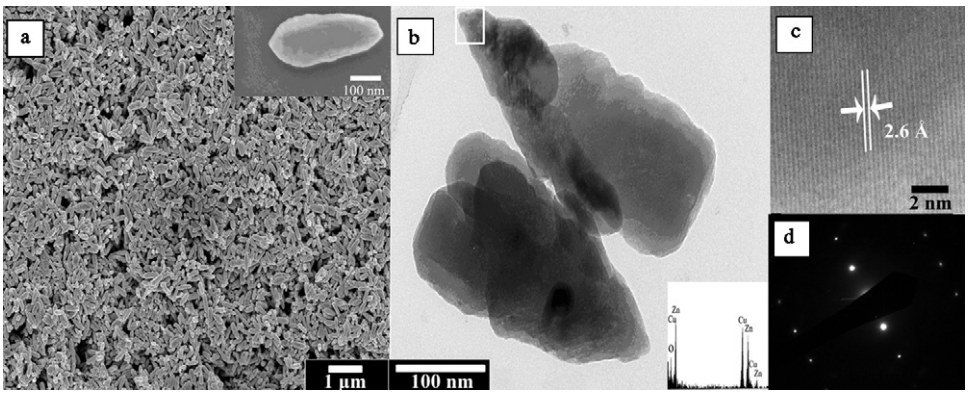

Fig. 2. (a) Low and high magnification (inset) SEM images of sample 1. (b) A typical TEM image. (c) HRTEM image taken from (b) and (d) SAED image of the ZnO nanobullet. (The inset of part (b) is its corresponding EDS spectrum.)

deficit, therefore, the growth along c-axis is greatly restrained. Notably, the single-crystalline nanobullets have much smaller lengths and diameters than those reported in literature previously [43], which appear to be generated by oriented aggregation of ZnO nanoparticles.

More characteristics of two samples were studied by Raman scattering and photofluorescence spectra. As shown in the Raman scattering spectra (Fig. 4), the two samples exhibit similar regions of the emission peaks under 514 nm excitation. The ZnO E_2 (high) phonon mode occurs at 436 cm^{-1}, and the peak at 331 cm^{-1} was assigned to multiple-phonon processes. Other peaks at 381 and 412 cm^{-1} corresponds to A1 (TO) and E1 (TO) of ZnO crystals respectively [47]. The absence of E1 (LO) peak around 580 cm^{-1} indicates the structural defects of the two samples since the E1 (LO) mode is associated with defects such as oxygen vacancy, zinc interstitials, or their complexes [48]. The corresponding photofluorescence is in good agreement with the conclusion. Fig. 5 illustrates room temperature photofluorescence (PL) spectra of ZnO nanobullets and nanoflakes under a photo excitation of 330 nm. The UV emission corresponds to the near band-edge emission, while the green emission peak at around 500 nm is commonly referred to as a deep-level or trap-state emission related to singly ionized oxygen vacancy [49–50].

The characteristic *J–V* curves of the DSSCs derived from nanobullets and nanoflakes have been comparatively investigated which are shown in Fig. 6. The resultant photovoltaic parameters are summarized in Table 1. The film thicknesses were controlled to be nearly the same of ~10 microns for

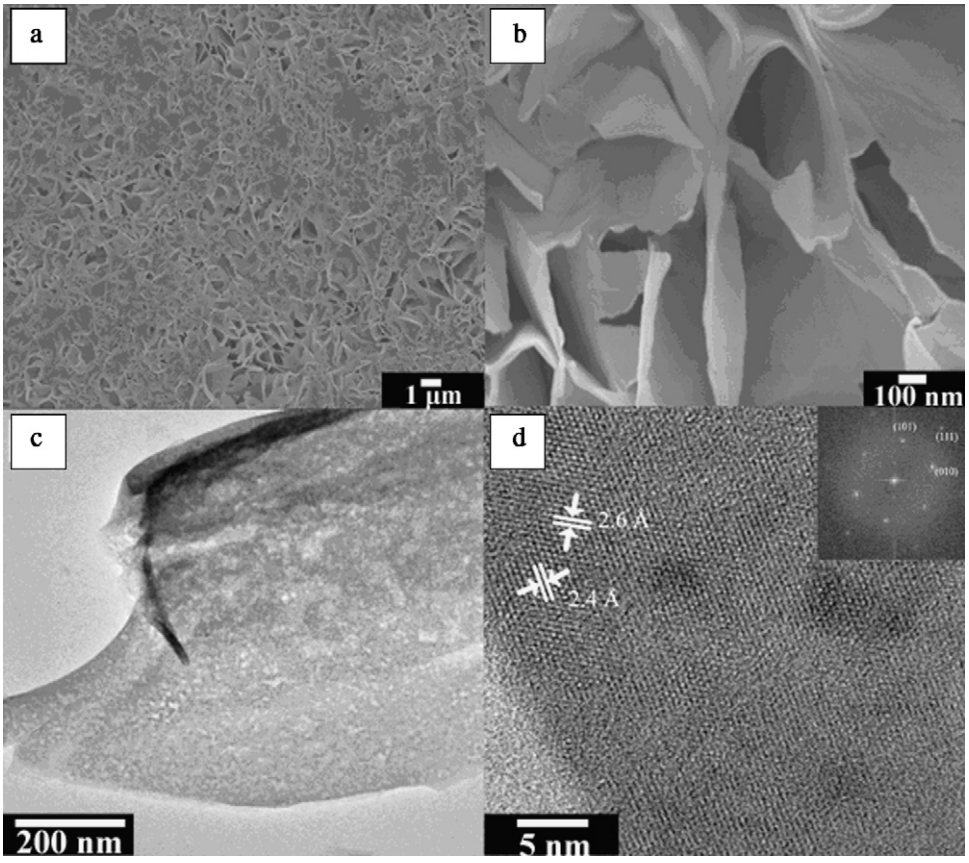

Fig. 3. (a) Low and high magnification, (b) SEM images of sample 2. (c) A typical TEM image, (d) HRTEM image. (The inset of part (d) is its corresponding fast Fourier transform (FFT) pattern).

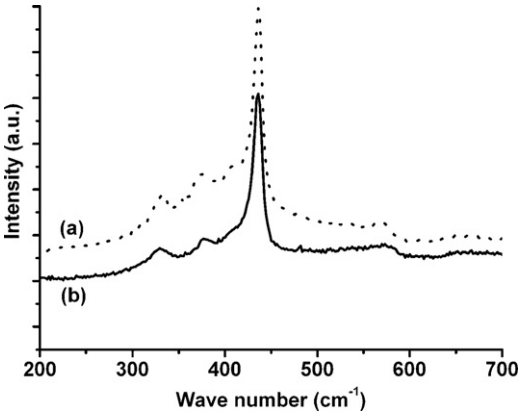

Fig. 4. Raman scattering spectra of nanobullets (a) and nanoflakes (b).

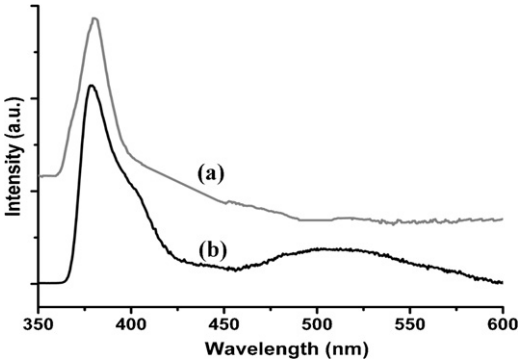

Fig. 5. Photofluorescence spectra of nanobullets (a) and nanoflakes (b).

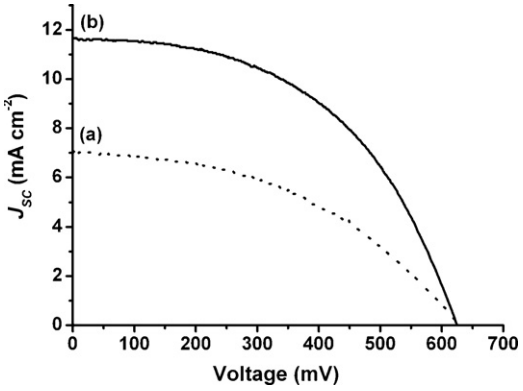

Fig. 6. Comparison of *J–V* curves of ZnO photoelectrodes based DSSCs. Nanobullets (a), nanoflakes (b).

both kinds of photoanodes. An overall conversion efficiency of 1.93% for a cell derived from nanobullets was achieved with J_{sc} = 7.0 mA cm^{-2}, V_{oc} = 629 mV, and *FF* = 43.8%. While a cell derived from nanoflakes achieved an overall energy conversion efficiency of 3.64% with J_{sc} = 11.6 mA cm^{-2}, V_{oc} = 624 mV, and *FF* = 50.2%, much higher than the performance of the cell derived from nanobullets. For a high-efficiency DSSC, a porous photoanode with a high internal surface area is essential for loading large amounts of dye molecules. The large increase in efficiency of nanoflakes derived DSSC than that of nanobullets derived one can be explained in terms of significant enhancement of optical absorption. The large surface area of the photoelectrode derived from nanoflakes causes an increment in the number of dye molecules adsorbed onto the ZnO surface. This is confirmed by the optical absorption studies as shown in Fig. 7. The spectra clearly show the increase in absorbance of the dye-modified film derived from nanobullets compared to that derived from nanoflakes, implying that a better light-harvesting efficiency can be obtained in the photoanode derived from nanoflakes. The light harvesting efficiency can be calculated from the equation LHE(λ) = 1–10$^{-\Gamma\sigma(\lambda)}$, where Γ is the surface concentration of dye molecules and σ is the absorption cross section. In order to determine the amount of dye molecules adsorbed in both of the photoanode films, the films were immersed in a 1 mM NaOH water/ethanol (1:1, v/v) solution for 24 h to make sure most of dyes were desorbed. Calculated from absorption spectra of the desorbed dye solutions, the values are 3.6 × 10^{-8} mol cm^{-2} for the film derived from nanobullets and 7.6 × 10^{-8} mol cm^{-2} for the film derived from nanoflakes, respectively. The results further demonstrate that the enhanced J_{sc} should be ascribed to the enhanced light harvesting due to increased dye adsorbing amount.

Table 1
Structural and performance characteristics of DSSCs based on photoanodes of sample 1 and sample 2.

DSSC	V_{oc} (mV)	J_{sc} (mA cm^{-2})	*FF* (%)	Efficiency (%)	Adsorbed dye (×10^{-8} mol cm^{-2})
DSC-1	629	7.0	43.8	1.93	3.6
DSC-2	624	11.6	50.2	3.64	7.8

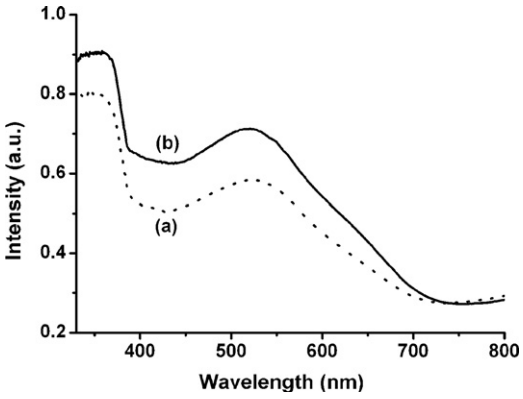

Fig. 7. Optical absorption spectra of two kinds of ZnO photoelectrode films. Nanobullets (a), nanoflakes (b).

4. Conclusions

In conclusion, we have successfully synthesized ZnO nanobullets/nanoflakes from zinc acetates by tuning the volume ratio between water and ethylene glycol solvent. The synthesis method is simple and can be easily scaled-up for mass production. The structural properties of the final products have been thoroughly studied by SEM, TEM, XRD, Raman scattering and photofluorescence spectra. Moreover, both kinds of ZnO production with distinct morphologies have been made as photoanodes in DSSC system. ZnO nanoflakes based DSSC has been demonstrated to possess much better performance (3.64% in efficiency) due to its larger dye adsorbing amount than that of nanobullets which is of 1.93% in efficiency. This work strongly emphasizes the importance of nanostructure in DSSC, and ZnO nanoplates has potential opportunity for the development of high efficient DSSC.

Acknowledgements

This work was supported by NSFC (No. 20771040) and Guangdong Science and Technology Department (No. 2008B050100017).

References

[1] M.H. Huang, Y. Wu, H. Feick, N. Tran, E. Weber, P. Yang, Adv. Mater. 13 (2001) 113–116.
[2] Z.W. Pan, Z.R. Dai, Z.L. Wang, Science 291 (2001) 1947–1949.
[3] J.T. Hu, T.W. Odom, C.M. Lieber, Acc. Chem. Res. 32 (1999) 435–445.
[4] S.D. Sharma, S.C. Kashyap, J. Appl. Phys. 42 (1971) 5302–5304.
[5] H. Iwanaga, N. Shibata, O. Nittono, M. Kasuga, J. Cryst. Growth 45 (1978) 228–232.
[6] Y.C. Kong, D.P. Yu, B. Zhang, W. Fang, S.Q. Feng, Appl. Phys. Lett. 78 (2001) 407–409.
[7] C.H. Liu, J.A. Zapien, Y. Yao, X.M. Meng, C.S. Lee, S.S. Fan, Y. Lifshitz, S.T. Lee, Adv. Mater. 15 (2003) 838–841.
[8] M.J. Zheng, L.D. Zhang, G.H. Li, W.Z. Shen, Chem. Phys. Lett. 363 (2002) 123–128.
[9] C.J. Lee, T.J. Lee, S.C. Lyu, Y. Zhang, H. Ruh, H.J. Lee, Appl. Phys. Lett. 81 (2002) 3648–3650.
[10] S.H. Jo, J.Y. Lao, Z.F. Ren, R.A. Farrer, T. Baldacchini, J.T. Fourkas, Appl. Phys. Lett. 83 (2003) 4821–4823.
[11] D. Banerjee, S.H. Jo, Z.F. Ren, Adv. Mater. 16 (2004) 2028–2032.
[12] G. Zhang, Q. Zhang, Y. Pei, L. Chen, Vacuum 77 (2004) 53–56.
[13] X. Wang, C.J. Summers, Z.L. Wang, Nano Lett. 4 (2004) 423–426.
[14] J.J. Wu, S.C. Liu, Adv. Mater. 14 (2002) 215–218.
[15] K. Yu, Y. Zhang, R. Xu, D. Jiang, L. Luo, Q. Li, Z. Zhu, W. Lu, Solid State Commun. 133 (2005) 43–47.
[16] J.Q. Hu, Q. Li, X.M. Meng, C.S. Lee, Chem. Mater. 15 (2003) 305–308.
[17] Y. Qiu, S. Yang, Adv. Funct. Mater. 17 (2007) 1345–1352.
[18] J.Q. Hu, Y. Bando, J.H. Zhan, Y.B. Li, T. Sekiguchi, Appl. Phys. Lett. 83 (2003) 4414–4416.
[19] C. Kim, Y. Kim, E. Jang, G. Yi, H. Kim, Appl. Phys. Lett. 88 (2006) 093104.
[20] S.J. Pearton, D.P. Norton, K. Ip, Y.W. Heo, T. Steiner, Prog. Mater. Sci. 50 (2005) 293–340.
[21] S. Musić, D. Dragčević, S. Popović, J. Alloys Compd. 429 (2007) 242–249.
[22] J.B. Baxter, E.S. Aydil, Appl. Phys. Lett. 86 (2005) 3114–3116.
[23] J.B. Baxter, E.S. Aydil, Sol. Energy Mater. Sol. Cells 90 (2006) 607–622.
[24] M. Law, L.E. Greene, J.C. Johnson, R. Saykally, P.D. Yang, Nat. Mater. 4 (2005) 455–459.
[25] M.E. Davis, Nature 417 (2002) 813–821.
[26] R. Katoh, A. Furube, K. Hara, S. Murata, H. Sugihara, H. Arakawa, M. Tachiya, J. Phys. Chem. B 106 (2002) 12957–12964.
[27] A. Furube, R. Katoh, T. Yoshihara, K. Hara, S. Murata, H. Arakawa, M. Tachiya, J. Phys. Chem. B 108 (2004) 12583–12592.
[28] B. O' Regan, M. Grätzel, Nature 353 (1991) 737–740.
[29] Y.J. Chen, M.C. Hsu, Y.C. Cai, J. Alloys Compd. 490 (2010) 493–498.
[30] Y.C. Qiu, W. Chen, S.H. Yang, Angew. Chem. Int. Ed. 49 (2010) 3675–3679.
[31] M.A. Green, K. Emery, D.L. King, Y. Hishikawa, W. Warta, Prog. Photovol.: Res. Appl. 14 (2006) 455–461.
[32] M. Grätzel, Inorg. Chem. 44 (2005) 6841–6851.
[33] Q. Zhang, T.P. Chou, B. Russo, S.A. Jenekhe, G. Cao, Adv. Funct. Mater. 18 (2008) 1654–1660.
[34] Q. Zhang, T.P. Chou, B. Russo, S.A. Jenekhe, G. Cao, Angew. Chem. Int. Ed. 47 (2008) 2402–2406.
[35] A.R. Ranga, V. Dutta, Nanotechnology 19 (2008) 445712.
[36] Y.C. Qiu, W. Chen, S.H. Yang, J. Mater. Chem. 20 (2010) 1001–1006.
[37] W. Chen, Y.C. Qiu, Y.C. Zhong, K.S. Wong, S.H. Yang, J. Phys. Chem. A 114 (2010) 3127–3138.
[38] A. Qurashi, M.F. Hossain, M. Faiz, N. Tabet, M. Alam, N.K. Reddy, J. Alloys Compd. 503 (2010) L40–L43.
[39] L.C. Damonte, V. Donderis, S. Ferrari, J. Orozco, M.A. Hernandez-Fenollosa, J. Alloys Compd. 495 (2010) 432–435.
[40] K.D. Yuan, X. Yin, J.T. Li, J.J. Wu, Y.M. Wang, F.Q. Huang, J. Alloys Compd. 489 (2010) 694–699.
[41] C.D. Lokhande, P.M. Gondkar, R.S. Mane, V.R. Shinde, S.H. Han, J. Alloys Compd. 475 (2009) 304–311.
[42] C.F. Lin, H. Lin, J.B. Li, X. Li, J. Alloys Compd. 462 (2008) 175–180.
[43] U.K. Gautam, L.S. Panchakarla, B. Dierre, X. Fang, Y. Bando, T. Sekiguchi, A. Govindaraj, D. Golberg, C.N.R. Rao, Adv. Funct. Mater. 19 (2008) 131–140.
[44] X. Zhou, Z.X. Xie, Z.Y. Jiang, Q. Kuang, S.H. Zhang, T. Xu, R.B. Huang, L.S. Zheng, Chem. Commun. 44 (2005) 5572–5574.
[45] C. Yan, D.F. Xue, J. Phys. Chem. B 110 (2006) 11076–11080.
[46] W. Peng, S. Qu, G. Cong, Z. Wang, Cryst. Growth Des. 6 (2006) 1518–1522.
[47] A.K. Pradhan, K. Zhang, G.B. Loutts, U.N. Roy, Y. Cui, A. Burger, J. Phys. Condens. Matter 16 (2004) 7123–7129.
[48] F.Q. He, Y.P. Zhao, Appl. Phys. Lett. 88 (2006) 193113.
[49] V.A. Roy, A.B. Djurišic, W.K. Chan, J. Gao, H.F. Lui, C. Surya, Appl. Phys. Lett. 83 (2003) 2253.
[50] J.B. Baxter, A.M. Walker, K. van Ommering, E.S. Aydil, Nanotechnology 17 (2006) S304–S312.